De-tensioning of collagen fibers optimizes endometrial receptivity and improves the rate of embryo implantation

Short title: **Collagen de-tensioning improves embryo implantation rate**

Eldar Zehorai[1†], Tamar Gross[1†], Elee Shimshoni[1], Ron Hadas[1], Idan Adir[1], Ofra Golani[2], Guillaume Molodij[2], Ram Eitan[3], Karl E. Kadler[4], Michal Neeman[1], Nava Dekel[1], Inna Solomonov[1*] and Irit Sagi[1*]

Affiliations

[1]Department of Biological Regulation, Weizmann Institute of Science, Rehovot 76100, Israel.

[2]Life Sciences Core Facilities, Weizmann Institute of Science, Rehovot 76100, Israel.
[3]Gynecologic Oncology Division, Helen Schneider Hospital for Women, Rabin Medical Center; Petah-Tikva and The Sackler Faculty of Medicine, Tel Aviv University, Tel Aviv, Israel.
[4]Wellcome Centre for Cell-Matrix Research, Faculty of Biology, Medicine and Health, Manchester Academic Health Sciences Centre, University of Manchester, Oxford Road, Manchester M13 9PT United Kingdom.

†Equal contribution
*Corresponding authors: inna.solomonov@weizmann.ac.il, irit.sagi@weizmann.ac.il

Abstract

Successful embryo implantation is associated with intensive endometrium matrix remodeling, in which fibrillar collagens and matrix metalloproteinases play a key role. Here we report that topical treatment with a single dose of human collagenase-1 improves the rate of embryo implantation in murine models regardless of genetic background. Collagenase-1 treatment reduces endometrial collagen-fiber tension affecting their aligned configuration while preserving the overall integrity of the uterine tissue. The collagenase treatment causes enhanced local vascular permeability and creates an inflammatory-like environment, all of which are necessary for successful embryo implantation. We show that this specific treatment rescued heat stress and embryo transfer induced embryo failure in mice. Our findings highlight the clinical feasibility to improve endometrial receptivity for embryo implantation. This treatment approach may be used to improve livestock breeding and for assisted human reproduction medical treatments.

Teaser

Mild specific collagen remodeling improves endometrial receptivity for natural and embryo-transfer-derived embryo implantation.

Introduction

Embryo implantation is a complex process consisting of dynamic genetic, biophysical and biochemical events in the uterine endometrium layer. For successful implantation, the endometrium is required to generate an appropriate microenvironment that is determined by many factors, including gene and hormonal expression, extracellular matrix (ECM) and local immune system reorganization, angiogenesis and others (*1-4*). There is a wide spectrum of mammalian endometrial responses to embryos of different qualities (*5-7*), and tightly regulated ECM remodeling plays a crucial role in establishing the optimal receptive conditions and synchronization of an appropriate embryo-endometrium cross-talk. This process takes place during each reproductive cycle to prime the endometrium for implantation, and continues during the window of implantation (WOI) and the decidualization phase (*8-11*).

During the embryo implantation period, the spatial and temporal expression of highly abundant endometrial collagens, types I, III, and V, are altered (*12-14*). In addition, due to intensive remodeling, collagen types I and III are locally reduced at the implantation sites in mice (*13, 14*). Similarly, the ultra-structure of fibrillar collagens in humans is changed during the first trimester of pregnancy (*15*). The data strongly indicate that fibrillar collagens play a role in trophoblast cell adhesion and invasion (*15-17*), whereas impaired remodeling of endometrial structural proteins is correlated with implantation failure and pregnancy loss (*18-23*). This suggests that highly regulated and targeted collagen remodeling may optimize the receptive state and improve conditions for successful implantation.

Endometrial remodeling during embryo implantation is mediated by various enzymes, most notable are matrix metalloproteinases (MMPs) (*11, 24-27*). MMPs are multifunctional proteases, which are able to degrade ECM proteins, shed cell surface receptors and activate biomolecules (*28, 29*). Successful embryo implantation requires a tight balance of their expression and proteolytic activity (*11, 24-27*). MMPs regulate trophoblast invasion (*9, 17, 30, 31*), and contribute to vascular remodeling, angiogenesis and inflammatory processes in the endometrium (*29, 32*). Studies have shown that MMP-1, 2, 3, 7, 9, 11 and 14 are involved in all stages of embryo

implantation and are expressed by both the endometrium and the trophoblast cells (*21, 24, 27, 33*). Yet, many of the specific functions of MMPs are unknown, this includes their role in regulating collagen reorganization at each stage of normal embryo implantation (*34*). Moreover, harnessing ECM remodeling mechanisms to promote normal tissue physiology, like implantation, remained largely unexplored.

Previously, we have demonstrated that specific proteolysis of collagen-rich ECM by collagenase-1 (MMP-1) leads to distinct combinatorial events that affect overall collagen morphology, ECM viscoelastic properties and molecular composition. These specific ECM changes uniquely affected cell morphologies, signaling patterns and gene-expression profiles. Specifically, we observed an improved ability of fibroblasts to adhere and invade collagen-rich ECM pretreated with collagenase-1 *ex vivo* (*35*). These observations motivated us to examine the effects of mild ECM remodeling, induced by collagenase-1 treatment, on embryo implantation.

Here, we demonstrate that a single topical administration of ~1µg of collagenase-1 was sufficient to improve embryo implantation rates in mice significantly, regardless of genetic background. Mechanistically, we revealed that this treatment induced mild alterations in spatial organization of collagen fibers, manifested in fiber de-tensioning that led to reduced fiber alignment. Additionally, we observed slightly enhanced angiogenesis, and signs of an inflammatory-like environment. Importantly, we did not detect intensive fibrillar degradation. The uterus preserved its structure and integrity and no indications of pathological hypervascularity and inflammation were observed. Mechanistically, our results show that the enhanced collagen de-tensioning optimizes endometrium receptivity and improves embryo implantation. In addition, this study highlights the potential utilization of collagenase-1-specific degradation for increasing success rates of embryo implantation, while providing new mechanistic insights into its important contribution to endometrial receptivity.

Results

Treatment with collagenase-1 improves the adherence of embryos *ex vivo* and implantation rate *in vivo*

Previously, we have shown that proteolysis of natural collagen fascicles from rat tendons by collagenase-1 leads to specific and unique ECM changes. Following collagenase-1 proteolysis, the fibril alignment was disrupted, producing a specific and robust degradation pattern, manifested in widely distributed broken and bent fibrils in multiple orientations (*35*). Further examination of the collagen network by scanning electron microscopy (SEM), revealed less packed, relaxed and disorganized collagen fibrils within each fiber. These observations signify the overall collagen fibers de-tension when treated by collagenase-1 (Fig. 1A).

As endometrial ECM-remodeling by MMPs is a crucial event for successful embryo implantation (*8, 11*), we hypothesized that inducing moderate remodeling of collagen fibers by collagenase-1 will positively affect the embryo-endometrium crosstalk. We therefore incubated mouse blastocysts with native collagen-rich ECM pretreated with either vehicle or collagenase-1 *ex vivo*. After 4 h of incubation, we observed more blastocysts on or in close proximity to the collagenase-1-treated matrix compared to the vehicle-treated matrix (Fig. 1B). This observation showed that collagen proteolysis enhances blastocyst-ECM interactions. This result prompted us to examine the effect of exogenous collagenase-1 treatment on embryo implantation rates *in vivo*. For this purpose, we used a spontaneous pregnancy model in which ICR copulated female mice were topically administered with ~1 µg of recombinant collagenase-1 or vehicle at day E2.5 (2.5 days post-coitum) (Fig. 1C). Embryo implantation sites were recorded 4 days later, at E6.5. A significant increase of ~60% in the number of embryo implantations was detected in the collagenase-1-treated mice (Fig. 1D). The same effect was observed in C57BL/6 mated females, demonstrating a significant improvement of ~50% in embryo implantation (Fig. S1). Littermates of treated animals were born healthy and viable, exhibiting normal development and behavior. Additionally, the weight of littermates measured 3 weeks after birth was within the range of the expected average weight of healthy mice of the same age and strain according to the literature (12±3 g) (*36*).

Topical administration of collagenase-1 does not affect tissue integrity

First, we set out to examine if mild collagenase-1 treatment affected the general structure of the endometrial tissue and its integrity at E4.5, which is the time when the embryo is fully attached and decidualization has begun. H&E staining at E4.5 demonstrates that all three tissue layers of the uterus after collagenase-1 treatment resemble the intact structure of the uteri in the control group. The myometrium and endometrium layers of the uteri were complete in both groups with clear segregating borders (Fig. 2A). In addition, the treatment did not affect the morphology of the luminal epithelium, which was organized as a simple-columnar monolayer with basal nuclei. Moreover, in the treated uteri, the typical tissue structures, such as endometrial glands, remained intact and were similar in appearance to the vehicle-treated uteri. Pathological examination further confirmed that there were no abnormalities or distinct morphological changes of cells within the uterus (epithelia, stroma, myometrium) following collagenase-1 treatment. To exclude the possibility of pathological trophoblast invasion to the myometrium as a result of collagenase-1 treatment, we examined the implantation site of GFP-expressing embryos within the uterine fibrillar collagens using two-photon microscopy with a second-harmonic generation (SHG) modality. The inspection was done at E6.5 when the invasion process is completed, and gastrulation starts. Figure 2B shows the representative images of GFP-embryos interacting only with collagens in the endometrium. Thus, mild amounts of collagenase-1 did not produce abnormal invasion depth of the implanted embryos.

Topical administration of collagenase-1 affects spatial organization of uterine collagen fibers

To investigate the mechanisms associated with the improvement in embryo implantation rates following collagenase-1 treatment, we examined collagen organization at different hierarchical levels before and during the window of implantation (WOI) i.e., days 2.5 and 4.5 post coitum, respectively.

First, we characterized the effect of collagenase-1 treatment on the organization of endometrial collagen fibers using SHG modality. This technique is a fast, convenient optical method, allowing visualization of collagen fiber assembly within the tissue. We imaged the fibers at E2.5 (i.e., 1 h post treatment) and at E4.5 (Fig. 3A, B). At both time points, the collagenase-1 treated uteri presented loosely packed and wavy fibers in comparison to the vehicle-treated uteri, which exhibited dense morphology with well-aligned and tightly packed collagen fibers. To assess

the degree of fiber dis-alignment, we subjected the images to unbiased orientation analysis, giving rise to the probability of collagen fibers orientations. The diversity of fiber orientations was measured by calculating the Shannon index, i.e., entropy of the distribution of orientations, as a non-parametric measure of distribution dispersion. The analysis revealed a slight, but significant increase in orientation entropy in treated compared to control uteri, both at 1h after treatment and at E4.5 (Fig. 3C, top). This result signifies the de-tensioning of collagen fibers induced by collagenase-1. Additional analysis of the area covered by collagen showed a trend of higher dense collagen organization in the vehicle group compared to collagenase-1 treated group (Fig. 3C, bottom). This density analysis indicates that the tissue becomes more permeable following collagenase-1 treatment, but gross fiber degradation does not take place. The image analysis indicated that the spatial disorganization of endometrial fibers induced by collagenase-1 last for at least two days. Next, we analyzed if the treatment with collagenase-1 affected the alignment of the myometrium collagen fibers. SHG images of cross-sections of uteri treated with vehicle or collagenase-1 showed no difference in directionality or area covered by collagen in both 1h and E4.5 samples (Fig. S2). This data confirms that the treatment by collagenase-1 did not affect the tension of collagen fibers in the myometrium.

High resolution scanning electron microscopy (SEM) imaging of E2.5 uteri collected 1h after collagenase treatment revealed distinct topological features of relaxed endometrium collagen fibers (Fig 3D). Their surface was covered by non-aligned wavy fibrils, indicating mild proteolysis of collagen. In contrast, the fibers in vehicle sample contained well-aligned densely packed collagen fibrils.

Next, we analyzed the three-dimensional microstructure of endometrium collagen fibrils using a high-resolution serial block-face scanning electron microscope (SBF-SEM). This VolumeEM modality provides sufficient resolution to study individual collagen fibrils by generating a representative reconstructed 3D model (*37*). Remarkably, the analysis of randomly selected reconstructed collagen fibrils (Fig. 3E), from samples taken 1 h after treatment, showed no changes in fibril volume fraction when compared to those of fibrils from vehicle samples (Fig. 3F). This analysis further indicated that no gross changes in fibril degradation had occurred following collagenase-1 treatment.

Taken together, the imaging analyses at different resolutions provides evidence that the mild proteolysis by collagenase-1 mostly manifests in de-tensioning of collagen fibers, affecting

collagen spatial organization, rather than intensive fibrils proteolysis. Such mild proteolysis increases tissue permeability, providing maternal structural support during the WOI.

Mild proteolysis induced by collagenase-1 promotes local vascular permeability

Successful embryo implantation relies on the induction of angiogenesis and uterine vascular permeability (*38-41*). To explore the angiogenic-related mechanisms associated with collagenase-1 treatment, magnetic resonance imaging (MRI) was applied at E4.5. The MRI signal enhancement was measured in the collagenase-1 and vehicle-treated samples during a period of ~30 min (Fig. 4A) to compare the accumulation of the contrast agent in the implantation sites. The contrast agent's concentration at each time point was normalized to its concentration in the vena cava, and normalized values were used to derive the MRI vascular parameters. Two main parameters characterizing vascular development and function were calculated: permeability surface area (PS) and fractional blood volume (fBV) (*38*). The analyses showed that implantation sites of uteri treated with collagenase-1 exhibited mild and not significant elevated PS and fBV values compared to implantation sites of vehicle-treated uteri (Fig. 4B,C). These MRI results indicate that collagenase-1 treatment induces a slight increase in local vascularization with no evidence of pathological hypervascularity. In addition, immunofluorescent imaging demonstrated that in response to collagenase-1 treatment, more of the injected contrast agents are observed accumulated within the implantation site (Fig. 4D). Taken together, these results indicate that the mild proteolysis of endometrium promotes local vascular permeability.

MRI results from E4.5 prompted us to look for mechanisms of increased angiogenesis. We tested the mRNA expression of *Kdr (Vegfr2)* and different isoforms of *Vegfa* at this time point, as they are the known players promoting angiogenesis in the uterus environment (*42-44*). Moreover, collagenase-1 is known to stimulate angiogenesis through vascular endothelial growth factor receptor 2 (VEGFR2) up-regulation (*45*). Our qRT-PCR analysis on E4.5 revealed a moderate increase in the transcription of *Vegfr2* (Fig. 5A) comparing collagenase-1 treated with vehicle. No increase in the mRNA level of *Vegf-a120, Vegf-a164 and Vegf-a188* isoforms were observed.

Previously we have shown that the degradation of collagen-rich ECM by collagenases accompanies the release of bioactive molecules (*35*). Since the qRT-PCR results did not show an increase in *Vegf-a* expression, we examined the direct effect of collagenase-1 on matrix-bound VEGF-A protein. For that, E2.5 uteri samples were completely decellularized and incubated with

the activated enzyme. Western blot analysis of the supernatant revealed a release of matrix-bound VEGF-A forms (i.e., VEGF-A164 and/or VEGF-A188) following incubation with collagenase-1. Remarkably, no VEGF-A release was detected in the vehicle-treated sample (Fig. 5B, S3). The release of the matrix-bounded VEGF-A proteins during mild proteolysis generates gradients of VEGF-A, which is a key initiation step in angiogenesis.

In addition, the protein levels of VEGFR2 in collagenase-1 treated samples were compared with vehicle at E4.5 and E6.5. Confirming the qRT-PCR results, we observed an increased trend in the expression of VEGFR2 at E4.5, which became significant in the later time point of E6.5 (Fig. 5C, S3). Likewise, staining of implantation sites after the WOI at E6.5 showed an increase in CD34 expression, which is a marker for angiogenesis (Fig. 5D).

Taken together, our results demonstrate the supportive role of collagenase-1 in the induction of angiogenic processes. First, mediated collagenolysis gives structural support for neovascularization. Second, collagenase-1 mediates induction of VEGFR2 and matrix-bound release of VEGF-A. This is accomplished without causing early pathological hyper-vascularization that can impair pregnancy outcomes (*46, 47*). Since embryo implantation relies on the induction of angiogenesis (*38-41*), the treatment with collagenase-1 allows a better supportive environment for embryo implantation.

Fiber de-tensioning induces NK cell infiltration and upregulation of the cytokine *Lif* required for embryo implantation

NK cells are the most abundant immune cells in the endometrium during embryo implantation, regulating trophoblast invasion, vascularization, and decidualization initiation (*3, 4*). In addition, intensive collagen degradation has been shown to promote immune cell migration (*48, 49*). Thus, we examined the effect of collagen de-tensioning on the infiltration of different immune cells into the treated endometrium. The flow cytometry analysis at E4.5 showed a specific increase of ~40% in NK cell population in treated mice, with no changes in T cell, dendritic cell, or macrophage populations (Fig. 6A,B, S4). Furthermore, western blot analysis at E4.5 of the NK cell marker (NKp46) confirmed the increase in the population of NK cells following treatment (Fig. 6D, S4A). Our results show that the de-tensioning of collagen following collagenase-1 treatment, leads to slight, but significant increase the infiltration of NK cells to the implantation site.

Since numerous cytokines and chemokines are involved in the crosstalk between the embryo and the endometrium (*3, 50, 51*), we compared the expression levels of several cytokines at E4.5 in both sample types. Following collagenase-1 treatment, a significant increase of Leukemia Inhibitor Factor (*Lif*), one of the most important pro-inflammatory cytokines involved in successful implantation (*52*), was detected at the transcript and protein level (Fig. 6D, S4A). Interestingly, there was no significant change in the expression levels of other tested cytokines (Fig. 6C).

A receptive endometrium has to exhibit typical signatures of tissue remodeling and inflammatory signaling. Our results show that collagenase-1 treatment promotes specific inflammatory signaling in the endometrium that is mild, but significantly stronger than in vehicle-treated mice. This inflammatory phenotype includes an increase in NK cell infiltration and *Lif* expression, where other important pro-inflammatory cytokines were not affected. Thus, the fiber de-tensioning by collagenase-1 improves the receptive state of the endometrium by promoting NK cell infiltration and *Lif* expression.

De-tensioning of collagen fibers by collagenase-1 improves implantation rate in heat stress and embryo transfer models

We determined the utility of collagenase-1 treatment in models in which embryo implantation has a lower success rate, i.e. heat stress and embryo transfer (ET) (*53-56*).

Prolonged elevated environmental temperature was reported to reduce successful pregnancy rates (*57, 58*). Accordingly, under heat stress conditions of 38 ºC, we observed a reduced embryo implantation rate with an average of 5 implantation sites per female (Fig. 7A,B). We hypothesized that the structural and signaling changes mediated by collagenase-1 treatment could compensate for the harmful effect of the elevated temperature. Indeed, treatment with collagenase-1 rescued the heat-stress effect as we observed 10.6 implantation sites per female on average (Fig. 7B). Notably, mouse body temperature during the heat-stress protocol remained at 36 ºC to 38 ºC, indicating the females were still in a normal and healthy physiological state (Fig. S5A).

Another well-known scenario with characteristically low implantation rates is the embryo transfer model (*56*). In humans, *in vitro* fertilization (IVF) and ET show relatively low pregnancy success rates mainly due to impaired implantation (*59-61*). Thus, we investigated whether

treatment with collagenase-1 can improve the implantation rate in a mouse embryo transfer model, in which blastocysts are transferred to a pseudo-pregnant female (female mated with a vasectomized male) (Fig. 7C). In this model, a significant two-fold increase in the number of embryo implantations was detected upon topical administration of recombinant collagenase-1 over control treatment (Fig. 7D). Furthermore, a similar increase in implantation rate following treatment was observed in a cross-strain embryo transfer protocol, in which cbcF1 embryos were transferred into ICR pseudo-pregnant females (Fig. S5B).

Altogether, these results show a general phenomenon in which endometrium-collagenase-1-mediated mild remodeling increases the number of implanted embryos regardless of their genetic background. Moreover, this gentle intervention is even able to override environmental stressors that impair the tightly controlled embryo implantation process.

The impact of collagenase-1 mild proteolysis on murine endometrial collagen reorganization and VEGF release is relevant for human uterine biology

A major intriguing question was the feasibility of our protocol to create mild collagen remodeling in assisted reproduction treatment protocols practiced in human females. To address this question, we explored if the treatment of human uteri samples with human collagenase-1 would display mechanisms similar to those observed in mice. Fresh endometrial biopsies from healthy women were excised, decellularized and incubated *ex vivo* either with collagenase-1 or vehicle and imaged under two-photon microscopy. Utilizing SHG imaging modality, we detected detension of collagen fibers in collagenase-1-treated endometrium layers similar to those observed in mice. Specifically, collagenase-1-treated endometrium layers displayed disaligned and loosely packed collagen fibers, in contrast to fibers in control samples (Fig. 7E). The effect of collagenase-1 on the release of vascularity formation factors, i.e., VEGF-A, from the ECM was also examined. As earlier described, after decellularization, the endometrial samples were incubated with either collagenase-1 or vehicle. An increased release of dimeric forms of VEGF-A was observed from the collagenase-1 treated matrices (Fig. 7F), similar to the results observed in murine samples (Fig. 5C). Overall, our results demonstrate that the effects induced by the mild proteolysis of collagenase-1 are similar in human and mouse tissues in terms of collagen morphology alteration and the release of pro-angiogenesis factors. These data indicate the potential use of a specific remodeling enzyme in human reproductive medicine.

Discussion

Embryo implantation outlines a critical phase of the reproductive process in mammals. Recent evidence suggests that this process is the main limiting factor for establishing natural early pregnancy and for the success of assisted reproductive techniques like *in vitro* fertilization–embryo transfer. Current studies show that successful embryo implantation requires both, a high quality embryo and a receptive endometrium microenvironment. Our results show that harnessing molecular aspects of mild and specific fibrillar endometrial collagens remodeling promotes key physiological processes that prime the uterus environment for successful embryo implantation. Specifically, we show that collagen de-tensioning induced in the endometrium by a single dose of collagenase-1 significantly improves embryo implantation success.

We assign this improvement to the proteolysis of native uteri collagen, which contributed mild collagen misalignment and release of angiogenic factors like VEGF-A. Together, these effects produce optimized endometrial microenvironment which promotes NK cell infiltration and neovascularization, which are necessary for successful embryo implantation. The specific biophysical and molecular mechanisms underlying the effect of collagenase-1 mediated collagen de-tensioning in improving embryo implantation are summarized in Fig. 8.

Due to the low success of assisted reproductive technology, many researchers occasionally investigated procedures associated with aspects of ECM remodeling to improve embryo implantation. Endometrial scratching is perhaps the most well-known strategy (*62*). The application of this method via biopsy prior to IVF procedure dramatically increases the chances of implantation by provoking inflammation and endometrial angiogenesis and was recommended by many clinicians prior to IVF (*63-65*). However, the efficiency of this procedure has been questioned by several studies (*66-68*). LIF administration was applied as another approach for increasing embryo implantation since this factor is dysregulated in infertile women suffering from recurrent implantation failure (*69, 70*). Unfortunately, the effect of LIF treatment was not as desired as it did not improve implantation rates and pregnancy outcomes for women with recurrent unexplained implantation failure. Another concept in improving embryo implantation focuses on enhancing vascularization. VEGF levels are significantly reduced in uterine fluid during the receptive phase in women with unexplained infertility compared with fertile women (*71*). Indeed, the study by Binder et al. showed that mouse embryos cultured with recombinant human VEGF (rhVEGF) had significantly higher implantation rates following blastocyst transfer compared with

control (*72*). However, the total effect of the rhVEGF on the uterus environment was not described. Taken together, these studies strongly indicate that manipulating factors associated with ECM remodeling have the potential to improve embryo implantation. However, the detailed mechanistic understanding of ECM remodeling mechanisms affecting the rate of embryo implantation is required. Collagen is the most abundant structural ECM molecule and it undergoes intensive remodeling during embryo implantation. We utilized the collagenolytic activity of collagenase-1 to loosen the extracellular matrix and thereby improve the receptivity of the endometrial microenvironment regardless of the embryo presence. Using a pseudo-pregnancy model at E4.5, we observed that collagenase-1 induces inflammatory and angiogenesis pathways independently from the presence of embryos (Fig. S6). These data strongly suggest that collagenase-1 primes the uterine environment for a successful embryo-endometrium dialogue. More importantly, the treatment was also able to rescue low implantation-rate scenarios in the heat-stress and embryo transfer models. Additionally, collagenase-1 administration does not affect the health of endometrial tissue or the offspring resulting from these pregnancies. The feasibility test of collagenase-1 application on human endometrial samples showed very similar mechanisms to those observed in mice, specifically, the spatial re-organization of collagen fibers and the release of VEGF-A. Our study highlights the potential of using the collagen remodeling enzyme collagenase-1 for livestock breeding and in assisted human reproductive protocols to overcome difficulties in both natural and IVF based embryo implantation.

Materials and Methods

MMP preparation and activation and enzymatic assays

Collagenase-1 was overexpressed and purified as described previously(*35*). Collagenase-1 was activated with 1 mM APMA (4-aminophenylmercuric acetate) in TNC buffer (50 mM Tris (pH 7.5), 150 mM NaCl, 10 mM $CaCl_2$) at 37 °C for 60 min. The enzymatic activity of collagenase-1 was measured at 37 °C by monitoring the hydrolysis of the fluorogenic peptide Mca-Pro-Leu-Gly-LeuDpa-Ala-Arg-NH2 at λex = 340 nm and λem = 390 nm as previously described (*73*).

Animals

All animals were obtained from Envigo Laboratories (Jerusalem, IL). On arrival, male mice were housed individually, and female mice were housed 3 to 5 per cage in animal rooms

maintained at 20 to 22 °C with an average relative humidity of 35% under a 12:12 h light: dark cycle and were housed in standardized ventilated microisolation caging. All experiments and procedures were approved by the Weizmann Institute of Science Animal Care and Use Committee (IACUC approval no. 27170516-2).

Administration of collagenase-1 or vehicle in a spontaneous pregnancy protocol

Female ICR or C57bl/6J mice (8-10 weeks old) were copulated with fertile ICR or C57bl/6J male mice (8-12 weeks old), respectively. Females which presented a vaginal plug on E0.5, were administered with l µg of recombinant collagenase-1 (l µg) or 1.5 µL of vehicle as control (TNC buffer) at E2.5 using the NSET™ Device of ParaTechs (Kentucky, US): mice were placed on a wire-top cage and allowed to grip the bars. The small and large specula were placed sequentially into the vagina to open and expose the cervix. Then, the NSET catheter was inserted through the large speculum, past the cervical opening, and into the uterine horn allowing the topical administration of recombinant collagenase-1 or vehicle. For generating fluorescent venus embryos, C57BL/6J female mice were mated with Myr-Venus homozygote males (*74*). Uteri were excised 1 h, 2 days or 4 days after treatment (E2.5, E4.5 and E6.5 respectively). On E4.5 and E6.5 the number of implantation sites was counted. On E6.5 implantation sites were visible and on E4.5 Evens-blue dye was injected intravenously 10 min before euthanizing which allows the visualization of the implantation sites.

Fascicle-derived ECM sample preparation

Fascicle-derived ECM was prepared from the tails of adult (6-mo-old) Norwegian rats. Specifically, rat tails were dissected, and tendon fascicles (diameter ~0.6 mm) were gently extracted and were washed extensively in TNC buffer to remove the macroscopic tissue debris and excess proteases. ECM samples were incubated with 500 nM collagenase-1 or vehicle (TNC) at 30 °C for 24 h.

Scanning electron microscopy (SEM)

Fascicle-derived ECM and E2.5 decellularized mouse uterus tissues were fixed in a 0.1-M cacodylate buffer solution (pH 7.4) containing 2.5% paraformaldehyde and 2.5% glutaraldehyde (pH 7.2) for 60 min at room temperature and then were washed three times in the same buffer. The

samples then were stained with 4% (wt/vol) sodium silicotungstate (Agar Scientific, UK) (pH 7.0) for 45 min with following dehydration through an ascending series of ethanol concentrations up to 100% ethanol. Next, the samples were dried in a critical point dryer (CPD) and attached to a carbon sticker. Finally, the samples were coated with thin gold/ palladium (Au/Pd) layer. The samples were observed under a Zeiss FEG Ultra55 SEM operating at 2 kV.

Seeding blastocysts on fascicle-derived ECM

Fascicle-derived ECM was incubated with 500 nM collagenase-1 in TNC or vehicle at 30°C for 24 h. Then, mouse blastocysts were seeded on top of the ECM. After 4 h of incubation, collagen and blastocysts were imaged.

De-cellularization of uterine tissue

E2.5 uteri samples treated with collagenase-1 or vehicle were incubated in a de-cell solution containing 3% Triton-100 (6 h, 4 °C) and then in a de-cell solution with 0.4% Triton-100 overnight at 4°C [de-cell solution: 1.5 M NaCl, 50 mM Tris pH 8, 50 mM EDTA, protease inhibitor cocktail (Roche)]. Samples were washed three times in ddH_2O and then incubated with 0.5% sodium deoxycholate (60 min, 25 °C) to remove lipid remaining. Samples were washed again three times in ddH_2O and stored at 4 °C until use.

H&E staining of frozen sections

E4.5 uteri samples treated with collagenase-1 or vehicle embedded in OCT were cross-sectioned (12μm) on glass microscope slides. Slides were washed with phosphate buffered saline (PBS) before staining. Then, slides were incubated in Hematoxylin for 3 min and washed with tap water. After, slides were dipped in 95% ethanol and incubated in Eosin for 45 sec. Next, samples were dipped in 95% ethanol and incubated 2 min in 100% ethanol. Finally, samples were incubated in xylene for 2 min and were mounted in mounting medium.

Two-photon microscopy and second-harmonic generation (SHG)

Snap-frozen murine uterine samples (excised at E2.5 and E4.5) were thawed in PBS, cut longitudinally, place on a slide as the endometrium facing up and covered with cover slip. Then samples were imaged using a two-photon microscope in a SHG mode (2PM:Zeiss LSM 510

META NLO; equipped with a broadband Mai Tai-HP-femtosecond single box tunable Ti-sapphire oscillator, with automated broadband wavelength tuning 700–1020 nm from Spectraphysics, for two-photon excitation). For second-harmonics imaging of collagen, a wavelength of 800-820 nm was used (detection at 390-450nm).

For imaging the myometrium layer, uteri samples embedded in OCT were cross-sectioned (50μm) on glass microscope slides.

Entropy analysis on the distribution of fiber orientations

Detection of collagen fibrils of vehicle and Collagenase-1 treated endometrium samples was performed using ImageJ (*75*). A mask highlighting collagen fibers was generated using the Tubeness plugin, and was followed by orientation analysis using the Directionality plugin (*76*). This gave rise to plots and spreadsheets of distribution of fiber orientations throughout the stacked images (Fig. S7, supplementary macrocode file named "Orientation"). Next, the orientation data was analyzed using Matlab. The degree of orientation diversity, i.e., distribution dispersion was measured by calculating the edge-orientation entropy that refers to the probability of encountering particular orientations in an image (*77*), and according to the Shannon index (*78*). For every orientation i, let p_i be the probability of the occurrence of orientation i in the image. Entropy or Shannon index (H') of the probability distribution is defined as $H' = -\sum_{i=-90}^{90} p_i \ln p_i$ (supplementary Matlab code file named "Entropy").

On E2.5 we analyzed 3 vehicle-treated females (4-12 images per each) and 5 collageanse-1-treated females (3-10 images per each). On E4.5 we analyzed 3 vehicle-treated females (4-16 images per each) and 3 collageanse-1-treated females (2-15 images per each).

Fibers density analysis

Fiber's density analysis was done by ImageJ software: For myometrium analysis, a single section was taken. For endometrium analysis a z-projection of max intensity was applied for 13 μm of the endometrium layer. For endometrium analysis only fibrillar areas were chosen. Next, auto threshold on the default setting was applied, and Analyze Particles plugin was used to detect the collagen-covered area. Size of particles was chosen as 0.172-infinity.

On E2.5 we analyzed 3 vehicle-treated females (4-12 images per each) and 5 collageanse-1-treated females (3-10 images per each). On E4.5 we analyzed 3 vehicle-treated females (4-16 images per each) and 3 collageanse-1-treated females (2-15 images per each).

SBF-SEM

Samples were prepared based on methods described previously (*37*). In brief, E2.5 uteri samples treated with collagenase-1 or vehicle were fixed in situ by using 2% (wt/vol) glutaraldehyde in 0.1 M phosphate buffer (pH 7), en-bloc stained in 2% (wt/vol) osmium tetroxide, 1.5% (wt/vol) potassium ferrocyanide in 0.1 M cacodylate buffer (pH 7.2), for 1h at 25ºC. Specimens were then washed again 5 x 3 min in ddH_2O and then specimens were placed in 2% osmium tetroxide in ddH_20 for 40 min at 25 ºC. Samples were then infiltrated and embedded in TAAB 812 HARD following sectioning using a Gatan 3View microtome within an FEI Quanta 250 SEM. For endometrium samples, a 41 μm × 41 μm field of view was chosen and imaged by using a 4096 × 4096 scan, section thickness was set to 100 nm in the Z (cutting) direction. Z volumes datasets comprised 700 images (100 μm z depth). The IMOD suite of image analysis software was used to build image stacks, reduce imaging noise, and generate 3D reconstructions. Fibrils were contoured using functions in the IMOD image analysis suite.

MRI imaging

MRI experiments were performed at 9.4 T on a horizontal- bore Biospec spectrometer (Bruker) using a linear coil for excitation and detection (Bruker) as reported previously (*38*). The animals were anesthetized with isoflurane (3% for induction, 1%–2% for maintenance; Abbott Laboratories) in 1 L/min oxygen, delivered through a muzzle mask. Respiration was monitored, and body temperature was maintained using a heated bed. The pregnant mice were serially scanned at E4.5. Three-dimensional gradient echo (3D-GE) images of the implantation sites were acquired before, and sequentially, for 30 min after i.v. administration of the contrast agent. A series of variable flip angle, precontrast T1-weighted 3D-GE images were acquired to determine the precontrast R1 (repetition time [TR]: 10 msec; echo time [TE]: 2.8 msec; flip angles 5°, 15°, 30°, 50°, 70°; 2 averages; matrix, 256 ′ 256 ′ 64; field of view [FOV], 35 ′ 35 ′ 35 mm3). Postcontrast images were obtained with a single flip angle (15°). During MRI experiments, the macromolecular contrast agent biotin-BSA-GdDTPA (80 kDa; Symo-Chem), 10 mg/mouse in 0.2 mL of PBS, was

injected i.v. through a preplaced silicone catheter inserted into the tail vein. The MRI scans allowed quantification of the fBV and the permeability surface area product (PS) of embryo implantation sites, as previously reported (*38*). In brief, the change in the concentration of the administered biotin-BSA-GdDTPA over time (Ct), in the region of interest, was divided by its concentration in the blood (Cblood); calculated in the region of interest depicting the vena cava, also acquired during MRI, and extrapolated to time 0). Linear regression of these temporal changes in Ct/Cblood yielded 2 parameters that characterize vascular development and function: (a) fBV (fBV = C0/Cblood), which describes blood-vessel density and is derived from the extrapolated concentration of the contrast agent in implantation sites, at time zero, divided by the measured concentration in the vena cava, approximately 5 min after i.v administration, and (b) PS = ([Ct – C0]/[Cblood ′ t]), which represents the rate of contrast agent extravasation from blood vessels and its accumulation in the interstitial space and which is derived from the slope of the linear regression of the first 15 minutes after contrast agent administration (t = 15). Mean fBV and PS were calculated separately for single implantation sites, considering homogeneity of variances between mice. At the end of the MRI session, embryo implantation sites were harvested and immediately placed in 4% PFA after sacrificing the pregnant mice by cervical dislocation. Slides were then washed in PBS and incubated in Cy3 or Cy2-conjugated streptAvidin (Jackson Immunoresearch Laboratories, PA, USA), diluted 1:150 in PBS for 45 min.

Immunofluorescence staining

Frozen Sections: Uterine samples embedded in OCT were cross-sectioned (10 µm) on glass microscope slides. Sections were fixed with PBS 4% paraformaldehyde (PFA) for 20 min at 25 ^{o}C. Samples were blocked in PBS, 20% normal horse serum, and 0.2% Triton x100 (20 min, 25 ^{o}C) and then incubated with a primary Ab in PBS, 2% normal horse serum, and 0.2% triton (overnight, 4 ^{o}C). Samples were then washed three times in PBS and incubated with a secondary antibody (60 min, 25 ^{o}C). Next, they were mounted in a mounting medium and covered with a cover slip. Primary antibodies: CD34 (CL8927PE; Cedarlane, Ontario, Canada).

Paraffin-Embedded Sections: Uterine samples were fixed with PBS 4% PFA, paraffin embedded and sectioned (4 µM). Slides were de-paraffinized using Wcap solution (Bio optica, Milano, Italy) (75 ^{o}C, 20 min). Antigen retrieval was performed in 0.1M EDTA, pH 8.0 (Diagnostic BioSystems, CA, USA) using a pressure cooker (125 ^{o}C, 3 min), followed by washes

with worm ddH_2O. Samples were blocked in PBS, 20% normal horse serum, and 0.2% Triton X-100 (20 min, 25 ^oC) and then incubated with primary Ab in PBS, containing 2% normal horse serumand 0.2% Triton X-100 (60 min, 25 ^oC).Next, samples were washed three times in PBS and incubated with a secondary antibody (60 min, 25 ^oC) and mounted in a mounting medium.

For each image, a suitable threshold was applied for CD34 channel, and Analyze Particles plugin was used to detect the covered area.

Quantitative Real Time PCR (qRT-PCR)

E4.5 uteri samples treated with collagenase-1 or vehicle were homogenized using a hand homogenizer. Total RNA was isolated using PerfectPure RNA Tissue Kit (5 Prime GmbH, Deutschland). 1 μg of total RNA was reverse transcribed using High Capacity cDNA Kit (Applied Biosystems inc. MA, USA). qRT-PCR was performed using specific primers with SYBR Green PCR Master Mix (Applied Biosystems inc.) on ABI 7300 instrument (Applied Biosystems) readouts were normalized to a B_2M housekeeping. Primer sequences are listed in Table 1 below. Data are presented as mean fold change using the $2^{-\Delta\Delta CT}$ method (*79, 80*). The standard error of the mean (SEM) was calculated on the $2^{-\Delta\Delta CT}$ data, as was the statistical analysis.

TABLE 1 | Primer sequences used for qRT-PCR.

Gene name	**Forward primer**	**Reverse primer**
B2m	CCCGCCTCACATTGAAATCC	GCGTATGTATCAGTCTCAGTGG
Lif	AACCAGATCAAGAATCAACTGGC	TGTTAGGCGCACATAGCTTTT
Il1a	CGCTTGAGTCGGCAAAGAAAT	TGGCAGAACTGTAGTCTTCGT
Il11	CTGCACAGATGAGAGACAAATTC	GAAGCTGCAAAGATCCCAATG
Tnf	AGGGATGAGAAGTTCCCAAATG	TGTGAGGGTCTGGGCCATA
Il1b	TTGACGGACCCCAAAAGATG	AGAAGGTGCTCATGTCCTCA
Ccl4	TTCCTGCTGTTTCTCTTACACCT	CTGTCTGCCTCTTTTGGTCAG
Cxcl12	CAGAGCCAACGTCAAGCA	AGGTACTCTTGGATCCAC
Kc	GCTGGGATTCACCTCAAGAA	CTTGGGGACACCTTTTAGCA

Vegfa (transcript 120)	CCCACGTCAGAGAGCAACAT	GGCTTGTCACATTTTTCTGGCT
Vegfa (transcript 164)	ACAAGGCTCACAGTGATTTTCT	CGTCAGAGAGCAACATCACC
Vegfa (transcript 188)	AGTTCGAGGAAAGGGAAAGG	GCCTTGGCTTGTCACATCT
Kdr (Vegfr2)	TGGACGGATGATCAAGAGAA	CTTCACAGGGATTCGGACTT

Cell extraction and western blotting

Frozen uterus tissues of 1 cm length were washed in PBS, homogenized in 0.5mL RIPA buffer (EMD Millipore, Burlington, MA, USA) with a protease inhibitor (Roche, Basel, Switzerland) using a hand homogenizer and centrifuged (14000 x*g*, 15 min, 4 ^{o}C). Supernatants were resuspended in sample buffer (200 mM Tris pH 6.8, 40% glycerol, 8% sodium dodecyl sulfate (SDS), 100 mM dithiothreitol (DTT), 0.2% bromophenol blue), and boiled for 5 min. Tissue extracts were then subjected to SDS polyacrylamide gel electrophoresis (PAGE) and transferred onto nitrocellulose membranes (Whatman, PA, USA) by electro-blotting. Membranes were blocked in Tris-buffered saline with Tween 20 (TBST) buffer (200 mM Tris pH 7.5, 1.5 M NaCl, 0.5% Tween 20) and 2% bovine serum albumin (BSA, 60 min, 25^{o}C) and then incubated with the corresponding primary Ab (60 min, 25 ^{o}C), washed three times with TBST and incubated with horseradish peroxidase (HRP)-conjugated secondary antibody (60 min, 25^{o}C). Quantification of the band intensities was performed using ImageJ analysis tool.

Antibodies used in this study: LIF (R&D systems, AF449), VEGF-R2 (cell signaling, 55B11), NKp46 (R&D systems, AF2225), β-tubulin (Santa cruz, sc-9104). Secondary antibodies (both anti-rabbit and mouse) conjugated to horseradish peroxidase (HRP) were purchased from Jackson ImmunoResearch (cat No.111-001-003 and 115-001-003, respectively). Antibodies were used at the manufacturer's recommended dilution.

Cell isolation from uterus tissue

Single implantation sites were stained using I.V injection of Evan's blue dye (Sigma-Aldrich, Rehovot, Israel), excised and isolated on E4.5. Tissues were minced into small fragments, and incubated in shaking for 40 min at 37 ^{o}C with 1 mL PBS (with Mg^{2+} and Ca^{2+}) containing 0.5

mg/mL collagenase type IV (Sigma-Aldrich, Rehovot, Israel) and 0.1 mg/mL DNase I (Roche). Digested tissue was filtered and smashed with a syringe plunger through a 250 μm nylon sieve in FACS buffer [PBS, 2% fetal calf serum (FCS), 2 mM ethylenediaminetetraacetic acid (EDTA)] to mechanically dissociate the remaining tissue. This was followed by three cycles of washing with FACS buffer at 30 x*g*, each time taking only the supernatant, while omitting the non-leukocyte cell pellet. The supernatant cell pellet was then centrifuged at 390 x*g*, and the pellet cells were lysed for erythrocytes using a red blood cell lysis buffer (Sigma-Aldrich, Rehovot, Israel) (2 min, 25 ºC).

Flow cytometry analysis

The following anti-mouse antibodies were used: CD45 (30-F11), CD3ε (clone 145-2C11), NKp46 (clone 29A1.4), NK1.1 (clone PK136), CD64 (clone 10.1), CD11b (clone M1/70), CD11c (clone N418), IAb (clone AF6-120.1) - all purchased from BioLegend (San Diego, USA). Anti-mouse F4/80 (clone A3-1) was purchased from BIORAD. The cells were incubated with the antibodies for 30 min in FACS buffer (dark, 4 ºC) and then washed once with FACS buffer. Cells were analyzed with BD LSR II, special order system (BD Biosciences). Flow cytometry analysis was performed using FlowJo software (TreeStar, Ashland, OR, USA).

Generating a pseudo-pregnant female mice

Pseudo-pregnant state in female mice was achieved accordingly: two ICR female mice (8-10 weeks old, minimum weight 26 gram) were placed with a vasectomized ICR male mouse (12 weeks old) in a single cage for mating. The female mice were checked the following morning (E0.5) for copulation plugs, and those with plugs were removed from the mating cage and housed together at 3-5 mice per cage.

Administration of collagenase-1 or vehicle in a heat stress protocol

Female ICR mice (8-10 weeks old) were copulated with fertile ICR male mice (8-12 weeks old). Females which presented a vaginal plug on E0.5, were administered with l μg of recombinant collagenase-1 or 1.5 μL of vehicle at E2.5 using the NSET™ Device of ParaTechs (Kentucky, US). After treatment, mice were transferred to preheated housing cages at 38 ºC for 4 days and were sacrificed at E6.5. Selected females were injected with a thermal microchip in the

back of the mice a week before the experiment. The microchip injection was done under an isoflurane sedation coupled with Carprofen (5 mg/kg) as an analgesic.

Administration of collagenase-1 or vehicle in a non-surgical embryo transfer (NSET) protocol

Pseudo-pregnant ICR mice (8-10 weeks old) at E2.5 were administered with l µg of recombinant collagenase-1 or 1.5 µL of vehicle using the NSET™ Device as describe above. After 15 min, embryos at the blastocyst stage were transferred also through the NSET catheter into the uterus (10 embryos per mice). Then, the device and specula were removed, and the mouse was returned to its home cage. Mice were allowed to recover in a clean cage for additional 4 days and the number of implanted embryos were counted and recorded on E6.5.

Human uterine samples

Uterine samples were obtained by Dr. Eitan Ram, Gynecologic Oncology Division, Helen Schneider Hospital for Women, Rabin Medical Center; Petah-Tikva. Helsinki approval no. 0450-16-RMC.

Statistical Analysis

Statistical analyses were carried out using GraphPad Prism software (VIII, GraphPad Software Inc., La Jolla, CA). Data were analyzed by unpaired, two-tailed t-test to compare between two groups. Multiple comparisons were analyzed by one-way analysis of variance (ANOVA). After the null hypothesis was rejected ($p < 0.05$), Tukey's Honestly Significant Difference or Dunnett tests were used for follow-up pairwise comparison of groups in the one-way ANOVA. Data are presented as mean ± SEM in the figures; values of $p < 0.05$ were considered statistically significant ($*P < 0.05$, $**P < 0.01$, $***P < 0.001$).

References

1. H. Cakmak, H. S. Taylor, Implantation failure: molecular mechanisms and clinical treatment. *Hum. Reprod. Update* **17**, 242-253 (2011).
2. J. Cha, X. Sun, S. K. Dey, Mechanisms of implantation: strategies for successful pregnancy. *Nat. Med.* **18**, 1754-1767 (2012).
3. M. S. Van Mourik, N. S. Macklon, C. J. Heijnen, Embryonic implantation: cytokines, adhesion molecules, and immune cells in establishing an implantation environment. *J. Leukoc. Biol.* **85**, 4-19 (2009).

4. Y. Gnainsky, N. Dekel, I. Granot, in *Seminars in reproductive medicine*. (Thieme Medical Publishers, 2014), vol. 32, pp. 337-345.
5. J. J. Brosens, M. S. Salker, G. Teklenburg, J. Nautiyal, S. Salter, E. S. Lucas, J. H. Steel, M. Christian, Y.-W. Chan, C. M. Boomsma, Uterine selection of human embryos at implantation. *Sci. Rep.* **4**, 1-8 (2014).
6. S. Quenby, G. Vince, R. Farquharson, J. Aplin, Recurrent miscarriage: a defect in nature's quality control? *Hum. Reprod.* **17**, 1959-1963 (2002).
7. N. S. Macklon, J. J. Brosens, The human endometrium as a sensor of embryo quality. *Biol. Reprod.* **91**, 98, 91-98 (2014).
8. B. A. Croy, A. T. Yamada, F. J. DeMayo, S. L. Adamson, *The guide to investigation of mouse pregnancy* (Academic Press, 2013).
9. J. Fata, A.-V. Ho, K. Leco, R. Moorehead, R. Khokha, Cellular turnover and extracellular matrix remodeling in female reproductive tissues: functions of metalloproteinases and their inhibitors. *Cell. Mol. Life Sci.* **57**, 77-95 (2000).
10. A. K. Sternberg, V. U. Buck, I. Classen-Linke, R. E. Leube, How Mechanical Forces Change the Human Endometrium during the Menstrual Cycle in Preparation for Embryo Implantation. *Cells* **10**, 2008 (2021).
11. T. E. Curry, Jr., K. G. Osteen, The matrix metalloproteinase system: changes, regulation, and impact throughout the ovarian and uterine reproductive cycle. *Endocr. Rev.* **24**, 428-465 (2003).
12. C. Oefner, A. Sharkey, L. Gardner, H. Critchley, M. Oyen, A. Moffett, Collagen type IV at the fetal–maternal interface. *Placenta* **36**, 59-68 (2015).
13. K. Spiess, W. R. Teodoro, T. M. Zorn, Distribution of collagen types I, III, and V in pregnant mouse endometrium. *Connect. Tissue Res.* **48**, 99-108 (2007).
14. H. Diao, J. D. Aplin, S. Xiao, J. Chun, Z. Li, S. Chen, X. Ye, Altered spatiotemporal expression of collagen types I, III, IV, and VI in Lpar3-deficient peri-implantation mouse uterus. *Biol. Reprod.* **84**, 255-265 (2011).
15. V. Sinai Talaulikar, K. Kronenberger, B. E. Bax, R. Moss, I. Manyonda, Differences in collagen ultrastructure of human first trimester decidua basalis and parietalis: implications for trophoblastic invasion of the placental bed. *J. Obstet. Gynaecol.* **40**, 80-88 (2014).
16. P. Xu, Y.-l. Wang, Y.-s. Piao, S.-x. Bai, Z.-j. Xiao, Y.-l. Jia, S.-y. Luo, L.-z. Zhuang, Effects of matrix proteins on the expression of matrix metalloproteinase-2,-9, and-14 and tissue inhibitors of metalloproteinases in human cytotrophoblast cells during the first trimester. *Biol. Reprod.* **65**, 240-246 (2001).
17. S. Shimonovitz, A. Hurwitz, M. Dushnik, E. Anteby, T. Geva-Eldar, S. Yagel, Developmental regulation of the expression of 72 and 92 kd type IV collagenases in human trophoblasts: a possible mechanism for control of trophoblast invasion. *AJOG* **171**, 832-838 (1994).
18. K. P. Conrad, M. B. Rabaglino, E. D. P. Uiterweer, Emerging role for dysregulated decidualization in the genesis of preeclampsia. *Placenta* **60**, 119-129 (2017).
19. C. M. Alexander, E. J. Hansell, O. Behrendtsen, M. L. Flannery, N. S. Kishnani, S. P. Hawkes, Z. Werb, Expression and function of matrix metalloproteinases and their inhibitors at the maternal-embryonic boundary during mouse embryo implantation. *Development* **122**, 1723-1736 (1996).
20. M. Rechtman, J. Zhang, L. Salamonsen, Effect of inhibition of matrix metalloproteinases on endometrial decidualization and implantation in mated rats. *Reproduction* **117**, 169-177 (1999).
21. E. Staun-Ram, S. Goldman, D. Gabarin, E. Shalev, Expression and importance of matrix metalloproteinase 2 and 9 (MMP-2 and -9) in human trophoblast invasion. *Reprod. Biol. Endocrinol.* **2**, 59 (2004).
22. C. L. Librach, Z. Werb, M. L. Fitzgerald, K. Chiu, N. M. Corwin, R. A. Esteves, D. Grobelny, R. Galardy, C. H. Damsky, S. J. Fisher, 92-kD type IV collagenase mediates invasion of human cytotrophoblasts. *J. Cell Biol.* **113**, 437-449 (1991).
23. P. Bischof, M. Martelli, A. Campana, Y. Itoh, Y. Ogata, H. Nagase, Importance of matrix metalloproteinases in human trophoblast invasion. *Early pregnancy: biology and medicine: The official journal of the Society for the Investigation of Early Pregnancy* **1**, 263-269 (1995).
24. L. Chen, M. Nakai, R. J. Belton, R. A. Nowak, Expression of extracellular matrix metalloproteinase inducer and matrix metalloproteinases during mouse embryonic development. *Reproduction* **133**, 405-414 (2007).
25. J.-Y. Zhu, Z.-J. Pang, Y.-h. Yu, Regulation of trophoblast invasion: the role of matrix metalloproteinases. *Rev. Obstet. Gynecol.* **5**, e137 (2012).
26. L. A. Salamonsen, Role of proteases in implantation. *Rev. Reprod.* **4**, 11-22 (1999).
27. J. Anacker, S. E. Segerer, C. Hagemann, S. Feix, M. Kapp, R. Bausch, U. Kämmerer, Human decidua and invasive trophoblasts are rich sources of nearly all human matrix metalloproteinases. *Mol. Hum. Reprod.* **17**, 637-652 (2011).

28. C. Bonnans, J. Chou, Z. Werb, Remodelling the extracellular matrix in development and disease. *Nat. Rev. Mol. Cell Biol.* **15**, 786-801 (2014).
29. Q. Chen, M. Jin, F. Yang, J. Zhu, Q. Xiao, L. Zhang, Matrix metalloproteinases: inflammatory regulators of cell behaviors in vascular formation and remodeling. *Mediat. Inflamm.* **2013**, (2013).
30. J. Chen, R. A. Khalil, Matrix metalloproteinases in normal pregnancy and preeclampsia. *Progress in molecular biology and translational science* **148**, 87-165 (2017).
31. K. Isaka, S. Usuda, H. Ito, Y. Sagawa, H. Nakamura, H. Nishi, Y. Suzuki, Y. Li, M. Takayama, Expression and activity of matrix metalloproteinase 2 and 9 in human trophoblasts. *Placenta* **24**, 53-64 (2003).
32. L. Nissinen, V. M. Kahari, Matrix metalloproteinases in inflammation. *Biochim. Biophys. Acta* **1840**, 2571-2580 (2014).
33. M. Cohen, A. Meisser, P. Bischof, Metalloproteinases and human placental invasiveness. *Placenta* **27**, 783-793 (2006).
34. M. Benkhalifa, Y. Zayani, V. Bach, H. Copin, M. Feki, M. Benkhalifa, M. Allal-Elasmi, Does the dysregulation of matrix metalloproteinases contribute to recurrent implantation failure? *Expert. Rev. Proteomics* **15**, 311-323 (2018).
35. I. Solomonov, E. Zehorai, D. Talmi-Frank, S. G. Wolf, A. Shainskaya, A. Zhuravlev, E. Kartvelishvily, R. Visse, Y. Levin, N. Kampf, D. A. Jaitin, E. David, I. Amit, H. Nagase, I. Sagi, Distinct biological events generated by ECM proteolysis by two homologous collagenases. *Proc. Natl. Acad. Sci. U.S.A.*, (2016).
36. T. Biosciences. (2021).
37. T. Starborg, N. S. Kalson, Y. Lu, A. Mironov, T. F. Cootes, D. F. Holmes, K. E. Kadler, Using transmission electron microscopy and 3View to determine collagen fibril size and three-dimensional organization. *Nat. Protoc.* **8**, 1433-1448 (2013).
38. V. Plaks, V. Kalchenko, N. Dekel, M. Neeman, MRI analysis of angiogenesis during mouse embryo implantation. *Magn. Reson. Med.* **55**, 1013-1022 (2006).
39. M. Kim, H. J. Park, J. W. Seol, J. Y. Jang, Y. S. Cho, K. R. Kim, Y. Choi, J. P. Lydon, F. J. DeMayo, M. Shibuya, VEGF‐A regulated by progesterone governs uterine angiogenesis and vascular remodelling during pregnancy. *EMBO Mol. Med.* **5**, 1415-1430 (2013).
40. D. S. Torry, J. Leavenworth, M. Chang, V. Maheshwari, K. Groesch, E. R. Ball, R. J. Torry, Angiogenesis in implantation. *J. Assist. Reprod. Genet.* **24**, 303-315 (2007).
41. D. Sherer, O. Abulafia, Angiogenesis during implantation, and placental and early embryonic development. *Placenta* **22**, 1-13 (2001).
42. S. B. Fournier, J. N. D'Errico, P. A. Stapleton, Uterine Vascular Control Preconception and During Pregnancy. *Compr. Physiol.* **11**, 1871-1893 (2021).
43. N. C. Douglas, H. Tang, R. Gomez, B. Pytowski, D. J. Hicklin, C. M. Sauer, J. Kitajewski, M. V. Sauer, R. C. Zimmermann, Vascular endothelial growth factor receptor 2 (VEGFR-2) functions to promote uterine decidual angiogenesis during early pregnancy in the mouse. *Endocrinology* **150**, 3845-3854 (2009).
44. X. Guo, H. Yi, T. C. Li, Y. Wang, H. Wang, X. Chen, Role of vascular endothelial growth factor (VEGF) in human embryo implantation: Clinical implications. *Biomolecules* **11**, 253 (2021).
45. R. Mazor, T. Alsaigh, H. Shaked, A. E. Altshuler, E. S. Pocock, E. B. Kistler, M. Karin, G. W. Schmid-Schönbein, Matrix metalloproteinase-1-mediated up-regulation of vascular endothelial growth factor-2 in endothelial cells. *J. Biol. Chem.* **288**, 598-607 (2013).
46. X. Chen, L. Jiang, C. C. Wang, J. Huang, T. C. Li, Hypoxia inducible factor and microvessels in peri-implantation endometrium of women with recurrent miscarriage. *Fertil. Steril.* **105**, 1496-1502. e1494 (2016).
47. B. Vailhé, J. Dietl, M. Kapp, B. Toth, P. Arck, Increased blood vessel density in decidua parietalis is associated with spontaneous human first trimester abortion. *Hum. Reprod.* **14**, 1628-1634 (1999).
48. D. E. Kuczek, A. M. H. Larsen, M.-L. Thorseth, M. Carretta, A. Kalvisa, M. S. Siersbæk, A. M. C. Simões, A. Roslind, L. H. Engelholm, E. Noessner, Collagen density regulates the activity of tumor-infiltrating T cells. *JITC* **7**, 1-15 (2019).
49. S. Goda, H. Inoue, H. Umehara, M. Miyaji, Y. Nagano, N. Harakawa, H. Imai, P. Lee, J. B. MaCarthy, T. Ikeo, Matrix metalloproteinase-1 produced by human CXCL12-stimulated natural killer cells. *Am. J. Pathol.* **169**, 445-458 (2006).
50. N. Dekel, Y. Gnainsky, I. Granot, K. Racicot, G. Mor, The role of inflammation for a successful implantation. *Am. J. Reprod. Immunol.* **72**, 141-147 (2014).
51. I. Granot, Y. Gnainsky, N. Dekel, Endometrial inflammation and effect on implantation improvement and pregnancy outcome. *Reproduction* **144**, 661-668 (2012).

52. S. J. Kimber, Leukaemia inhibitory factor in implantation and uterine biology. *Reproduction* **130**, 131-145 (2005).
53. P. J. Hansen, Effects of heat stress on mammalian reproduction. *Philos. Trans. R. Soc. Lond., B, Biol. Sci.* **364**, 3341-3350 (2009).
54. K. A. Wani, J. Irfan, J. A. Malik, "Impact of Heat Stress on Embryonic Implantation" in *Climate Change and Its Impact on Fertility* (IGI Global, 2021), pp. 99-112.
55. A. Aggarwal, R. Upadhyay, *Heat stress and animal productivity* (Springer, 2013), vol. 188.
56. K. Wakuda, K. Takakura, K. Nakanishi, N. Kita, H. Shi, M. Hirose, Y. Noda, Embryo-dependent induction of embryo receptivity in the mouse endometrium. *Reproduction* **115**, 315-324 (1999).
57. K. Y. B. Ng, R. Mingels, H. Morgan, N. Macklon, Y. Cheong, In vivo oxygen, temperature and pH dynamics in the female reproductive tract and their importance in human conception: a systematic review. *Hum. Reprod. Update* **24**, 15-34 (2018).
58. F. Marco‐Jiménez, C. Naturil‐Alfonso, D. Peñaranda, E. Jiménez‐Trigos, F. J. García‐Diego, J. Vicente, Maternal Exposure to High Temperatures Disrupts OCT 4 mRNA Expression of Rabbit Pre‐Implantation Embryos and Endometrial Tissue. *Reprod. Domest. Anim.* **48**, 429-434 (2013).
59. E. J. Forman, K. H. Hong, K. M. Ferry, X. Tao, D. Taylor, B. Levy, N. R. Treff, R. T. Scott Jr, In vitro fertilization with single euploid blastocyst transfer: a randomized controlled trial. *Fertil. Steril.* **100**, 100-107. e101 (2013).
60. L. Mains, B. J. Van Voorhis, Optimizing the technique of embryo transfer. *Fertil. Steril.* **94**, 785-790 (2010).
61. M. Cozzolino, A. Vitagliano, M. V. Di Giovanni, A. S. Laganà, S. G. Vitale, M. Blaganje, K. D. Starič, K. Borut, T. S. Patrelli, M. Noventa, Ultrasound-guided embryo transfer: summary of the evidence and new perspectives. A systematic review and meta-analysis. *Reprod. Biomed. Online* **36**, 524-542 (2018).
62. D. N. Barash A, Fieldust S, Segal I, Schechtman E, Granot I. , Local injury to the endometrium doubles the incidence of successful pregnancies in patients undergoing in vitro fertilization. *Fertil Steril.* **79**, 1317-1322 (2003).
63. C. Siristatidis, N. Vrachnis, P. Vogiatzi, C. Chrelias, A. Q. Retamar, S. Bettocchi, D. Glujovsky, Potential pathophysiological mechanisms of the beneficial role of endometrial injury in in vitro fertilization outcome. *Reprod. Sci.* **21**, 955-965 (2014).
64. J.-H. Yang, C.-D. Chen, C.-H. Chou, W.-F. Wen, P.-N. Tsao, H. Lee, S.-U. Chen, Intentional endometrial injury increases embryo implantation potentials through enhanced endometrial angiogenesis. *Biol. Reprod.* **100**, 381-389 (2019).
65. Y. Gnainsky, I. Granot, P. B. Aldo, A. Barash, Y. Or, E. Schechtman, G. Mor, N. Dekel, Local injury of the endometrium induces an inflammatory response that promotes successful implantation. *Fertil. Steril.* **94**, 2030-2036 (2010).
66. N. Van Hoogenhuijze, J. Kasius, F. Broekmans, J. Bosteels, H. Torrance, Endometrial scratching prior to IVF; does it help and for whom? A systematic review and meta-analysis. *Hum. Reprod. Open* **2019**, hoy025 (2019).
67. X. Santamaria, N. Katzorke, C. Simón, Endometrial 'scratching': what the data show. *Curr. Opin. Obstet. Gynecol.* **28**, 242-249 (2016).
68. S. Lensen, D. Osavlyuk, S. Armstrong, C. Stadelmann, A. Hennes, E. Napier, J. Wilkinson, L. Sadler, D. Gupta, A. Strandell, A randomized trial of endometrial scratching before in vitro fertilization. *NEJM* **380**, 325-334 (2019).
69. P. R. Brinsden, V. Alam, B. de Moustier, P. Engrand, Recombinant human leukemia inhibitory factor does not improve implantation and pregnancy outcomes after assisted reproductive techniques in women with recurrent unexplained implantation failure. *Fertil. Steril.* **91**, 1445-1447 (2009).
70. E. Hambartsoumian, Endometrial leukemia inhibitory factor (LIF) as a possible cause of unexplained infertility and multiple failures of implantation. *Am. J. Reprod. Immunol.* **39**, 137-143 (1998).
71. N. Hannan, P. Paiva, K. Meehan, L. Rombauts, D. Gardner, L. Salamonsen, Analysis of fertility-related soluble mediators in human uterine fluid identifies VEGF as a key regulator of embryo implantation. *Endocrinology* **152**, 4948-4956 (2011).
72. N. K. Binder, J. Evans, D. Gardner, L. A. Salamonsen, N. J. Hannan, Endometrial signals improve embryo outcome: functional role of vascular endothelial growth factor isoforms on embryo development and implantation in mice. *Hum. Reprod.* **29**, 2278-2286 (2014).
73. C. G. Knight, F. Willenbrock, G. Murphy, A novel coumarin‐labelled peptide for sensitive continuous assays of the matrix metalloproteinases. *FEBS Lett.* **296**, 263-266 (1992).

74. J. M. Rhee, M. K. Pirity, C. S. Lackan, J. Z. Long, G. Kondoh, J. Takeda, A. K. Hadjantonakis, In vivo imaging and differential localization of lipid ‐ modified GFP ‐ variant fusions in embryonic stem cells and mice. *Genesis* **44**, 202-218 (2006).
75. A.-C. I. Schindelin J, Frise E, Kaynig V, Longair M, Pietzsch T, Preibisch S, Rueden C, Saalfeld S, Schmid B, Tinevez JY, White DJ, Hartenstein V, Eliceiri K, Tomancak P, Cardona A., Fiji: an open-source platform for biological-image analysis. *Nat. Methods* **9**, 676-682 (2012).
76. Z.-Q. Liu, Scale space approach to directional analysis of images. *Appl. Opt.* **30**, 1369-1373 (1991).
77. M. Grebenkina, Brachmann, A., Bertamini, M., Kaduhm, A., Redies, C., Edge-Orientation Entropy Predicts Preference for Diverse Types of Man-Made Images. *Front. Neurosci.* **12**, 678 (2018).
78. C. E. Shannon, A mathematical theory of communication. *Bell Syst. tech. j.* **27**, 379-423 (1948).
79. K. J. Livak, T. D. Schmittgen, Analysis of relative gene expression data using real-time quantitative PCR and the 2− ΔΔCT method. *Methods* **25**, 402-408 (2001).
80. T. D. Schmittgen, K. J. Livak, Analyzing real-time PCR data by the comparative CT method. *Nat. Protoc.* **3**, 1101-1108 (2008).

Acknowledgments: We thank Dr. Alina Berkovitz for embryo preparations and fruitful discussions, Ms Anna Aloshin for collagenase-1 purification, and Ms Yinhui Lu at the University of Manchester for collecting SBF-SEM images. We thank Dr. Ori Brenner for assistance in histopathological characterization of mice uteri. The images in this paper were acquired at the Optical Imaging & Translational Bioengineering Unit, Department of Veterinary Resources, and at the Advanced Optic Imaging Unit, de Picciotto-Lesser Cell Observatory In memory of Wolfgang and Ruth Lesser at the Moross Integrated Cancer Center Life Science Core Facilities, Weizmann Institute of Science.

Funding: IS is the Incumbent of the Maurizio Pontecorvo Professorial Chair and has received funding from the Israeli Science Foundation (1226/13), European Union's Horizon 2020 research and innovation programme (grant agreement No [801126]), Eu 2020 EDIT consortium, Cynthia and Andrew Adelson fund, The Mireille & Murray Steinberg Family Foundation, The Thompson Family Foundation, the German-Israeli Foundation for Scientific Research and Development (GIF), the European Research Council AdG (THZCALORIMETRY-DLV-695437) and the USAIsrael Binational Science Foundation (71250601), the Ambach fund, and the Kimmelman center at the WIS.

Author contributions: Conceptualization: EZ, ISo, ISa; Investigation: EZ, TG, ES, GM, KEK, ISo, ISa; Methodology: EZ, TG, ES, RH, OG, GM, KEK, MN, ND Validation: EZ, ES, RH, IA, GM, OG, ISo; Visualization: EZ, TG, RH; Formal analysis: EZ, TG, RH, IA; Resources: RE,

KEK, MN; Supervision: ISo, ISa; Writing - original draft: ED, TG, ISo,ISa; Writing—review & editing: TG, ISo, EZ, IA, KEK, ES; RH, GM, OG, MN, ND, ISa; Funding acquisition: ISa.

Competing interests: "Compositions for remodeling extracellular matrix and methods of use thereof" (U.S. patent no. 10722560). Assignee: NanoCell Ltd, Investors: ISa, ISo, EZ. All other authors declare that they have no competing interests.

Data and materials availability: All data needed to evaluate the conclusions in the paper are available in the main text or the supplementary materials.

Figures and Tables

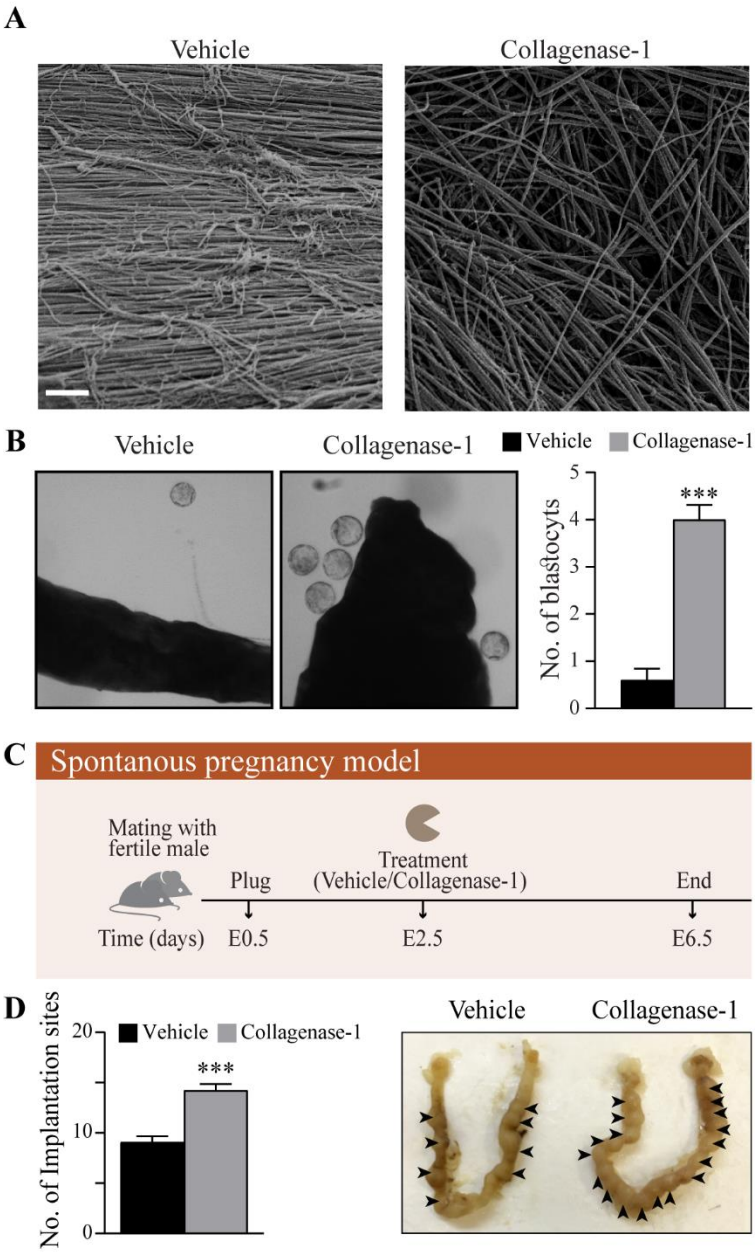

Fig. 1. Treatment with collagenase-1 improves the adherence of embryos *ex-vivo* and implantation rate *in-vivo*. **(A)** Representative SEM images of native rat tail collagen fiber pretreated with collagenase-1 or vehicle. The mild treatment with collagenase-1 affects fibrils alignment within the fiber. **(B)** Representative images of native rat tail collagen fiber pretreated with collagenase-1 or vehicle and then incubated with blastocysts for 4 h. Blastocysts that were in close proximity to the collagen were counted (n = 5). **(C)** Schematic representation of the spontaneous pregnancy model. **(D)** Quantification of implantation sites and representative images of the uteri at E6.5. Implantation sites marked by arrowheads (n = 30). Data were analyzed by an unpaired, two-tailed t-test. Results are presented as mean ± SEM with significance: ***$p < 0.001$.

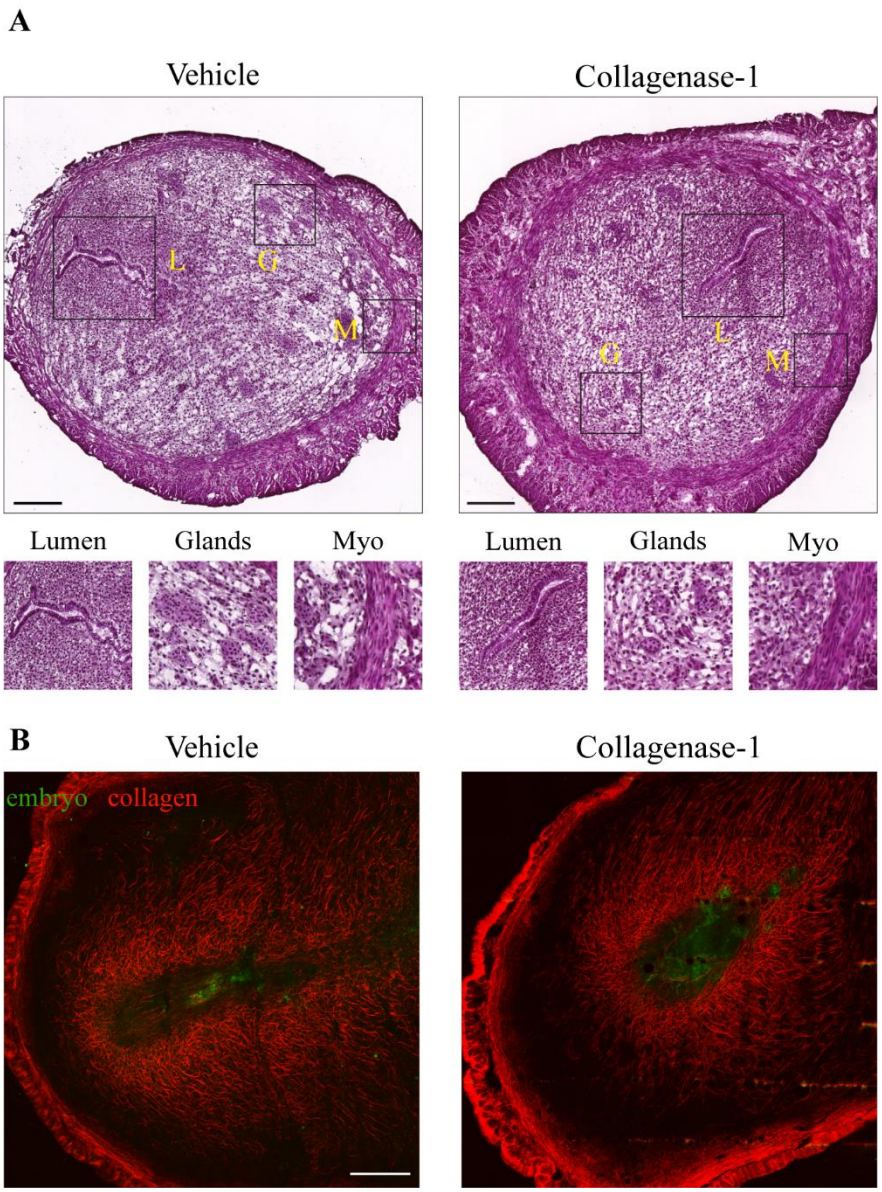

Fig. 2. Topical administration of collagenase-1 does not result in disruption of tissue integrity or over invasiveness of the embryo. (A) Representative H&E images of uteri at E4.5 (n = 3). The myometrium and endometrium layers of the uteri are seen intact in both groups. The treatment did not affect the morphology of the luminal epithelium, endometrial glands and myometrium. **(B)** Representative SHG images of transverse uteri sections of vehicle and collagenase-1 treated mice at E6.5, show that collagenase-1 treatment did not affect embryo invasiveness (green: venus-embryo, red: collagen fibers) (scale bar = 50 μm) (n = 1).

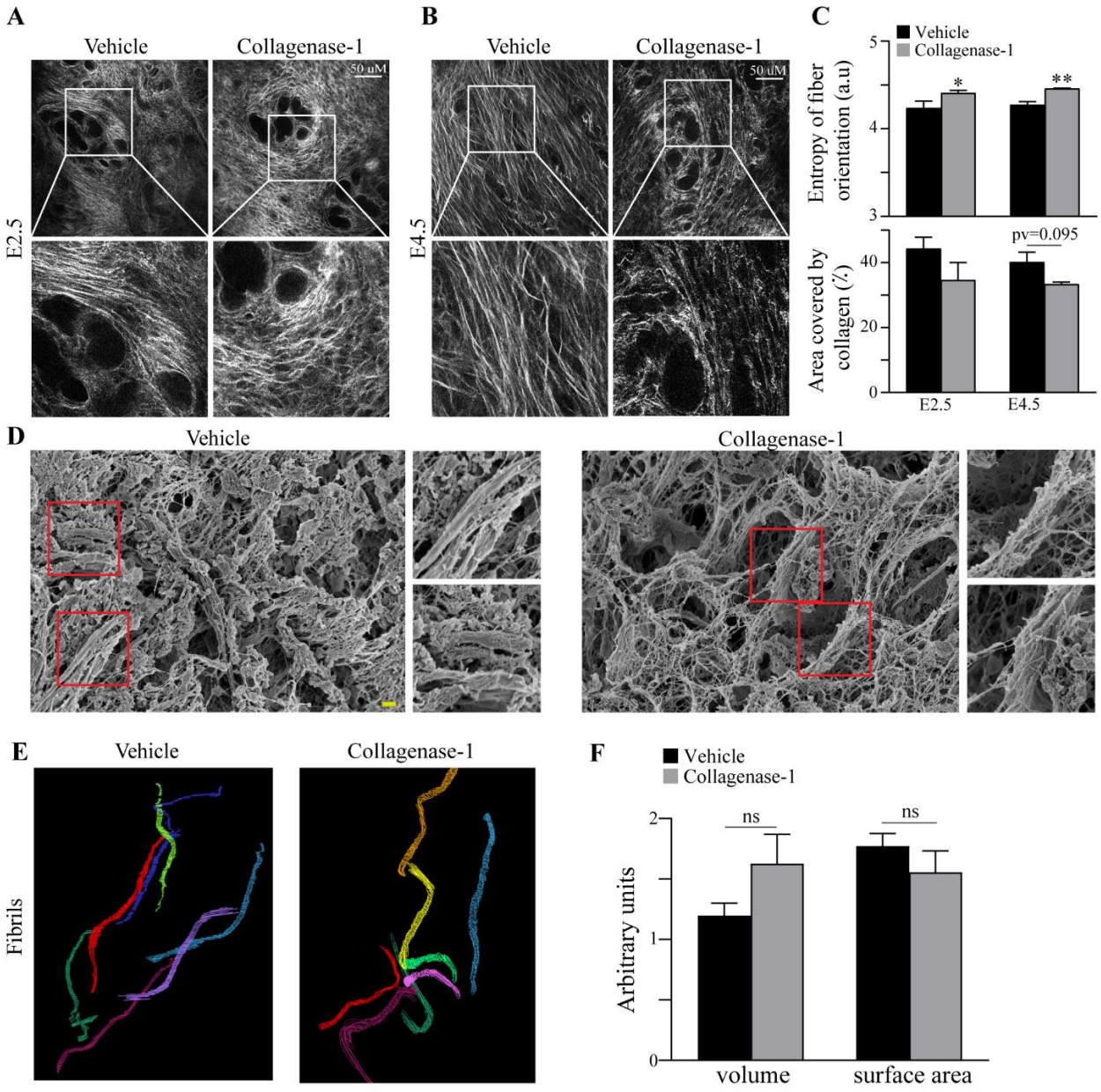

Fig. 3. Topical administration of collagenase-1 results in the modification of the spatial organization of uterine collagen fibrils. (A, B) Representative SHG images of longitudinal sections vehicle- and collagenase-1 treated uterine samples at E2.5 (1h after treatment) and E4.5, respectively. Only the endometrium layer is imaged, scale bar = 50 µM, (n≥3). **(C)** Measurements of the entropy of fibers orientation (top), and area covered by collagen (bottom). Analysis was done using ImageJ software. **(D)** Representative SEM images of endometrial layers vehicle- and collagenase-1-treated, 1h after the treatment. The images display well-aligned dense fibril packing on fiber surfaces of vehicle samples *vs* dis-aligned wavy fibrils on the fiber surfaces of treated samples, scale bar=1µm. **(E)** Representative 3D reconstructions from serial block face-VolumeEM analysis of endometrium fibrils of vehicle- and collagenase-1-treated uteri. **(F)** Analyses of volume and surface area of fibrils from vehicle- and collagenase-1- treated uteri does not show the significant difference (n = 8 fibrils), indicating the absence of massive fibril degradation. Data were

analyzed by an unpaired, two-tailed t-test. Results are presented as mean ± SEM with significance: *p < 0.05, ** p-value <0.01.

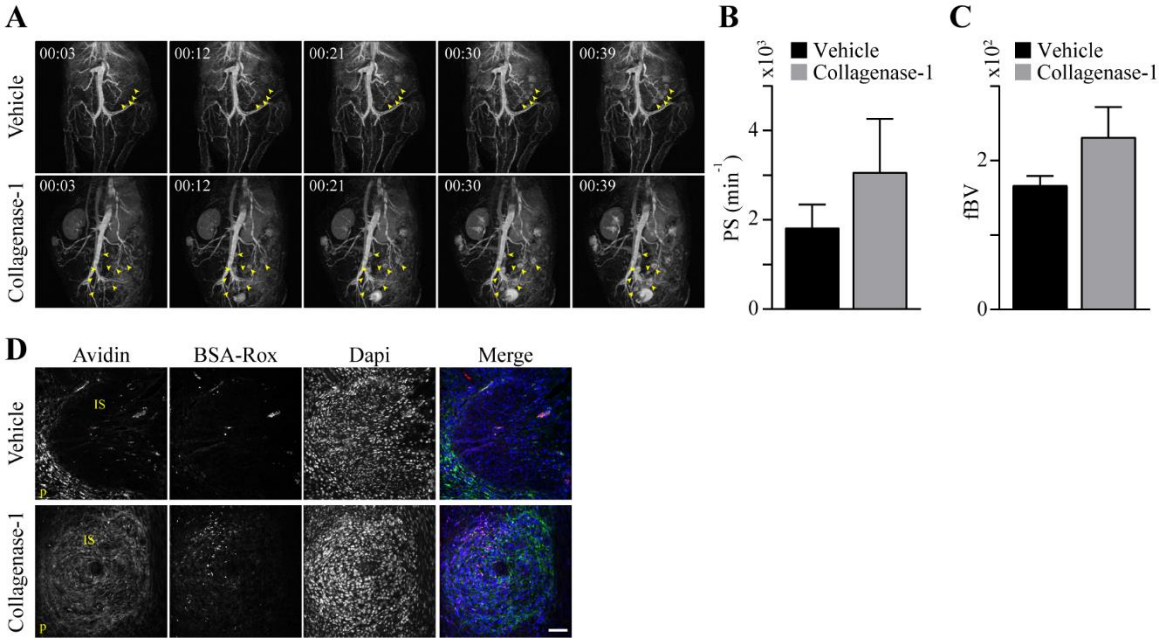

Fig. 4. Collagenase-1 enhances blood vessel permeability at implantation sites. (A) Representative MRI images at E4.5 of vehicle- and collagenase-1-treated uteri. Arrows indicate implantation sites. **(B)** Quantification of the permeability surface at implantation sites, taken from the MRI data (n = 7). **(C)** Quantification of the fractional blood volume (fbv) at implantation sites, taken from the MRI data (n = 7; 9.4T, 3D GE; IV biotin-BSA-GdDTPA). **(D)** Immunofluorescence imaging of the contrast agents: biotin-BSA-Gd-DTPA and BSA-Rox, demonstrating their accumulation in the implantation sites during MRI imaging for 30 and 2.5 min, respectively. Data were analyzed by an unpaired, two-tailed t-test. Results are presented as mean ± SEM.

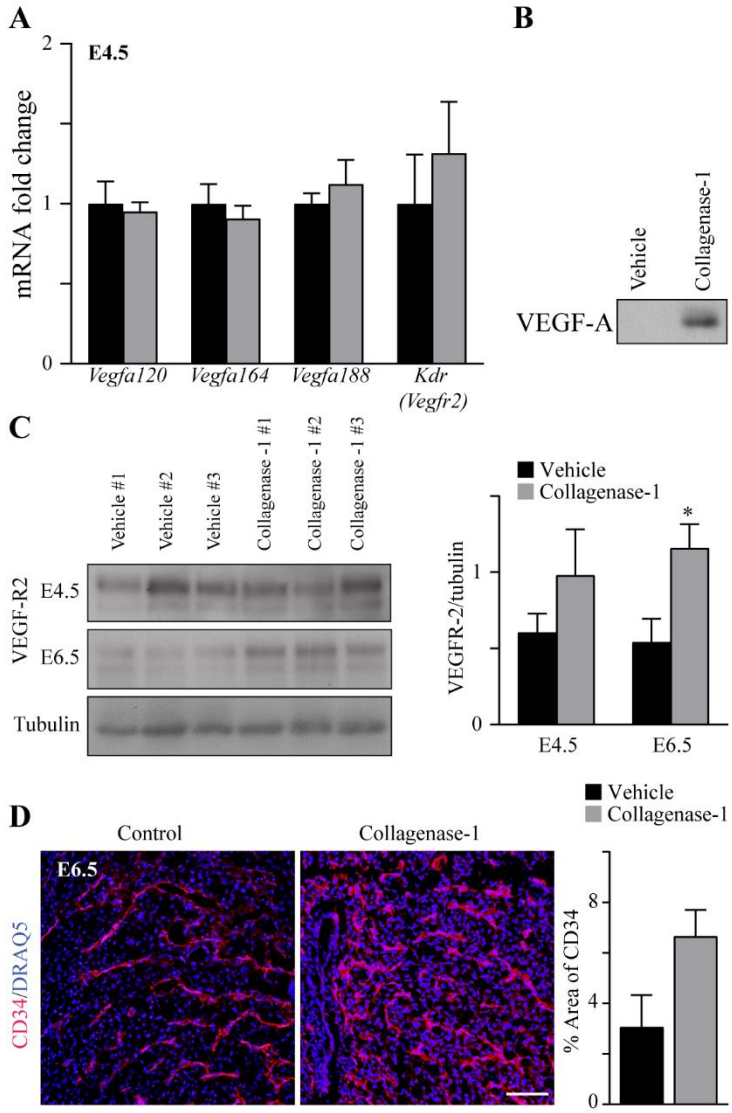

Fig. 5. Collagenase-1 promotes vascular permeability at implantation sites. (A) Real-time PCR transcription analysis of angiogenic factors at E4.5 ($n \geq 7$). **(B)** Representative western blot analysis show protein expression of VEGF-A in supernatants from decellularized uterus samples that were incubated with collagenase-1 or vehicle for 24 h. **(C)** Western blot analysis shows the increase of VEGF-R2 levels in E4.5-6.5 samples treated with collagenase-1 (left). This difference becomes to be significant at E6.5. Quantification of protein expression shown in C, using ImageJ analysis tool (right) ($n = 3$). **(D)** Representative images of immunofluorescent staining against CD34 of E6.5 samples. Covered area quantification was performed using ImageJ analysis tool. Data were analyzed by an unpaired, two-tailed t-test. Results are presented as mean ± SEM with significance: $*p < 0.05$.

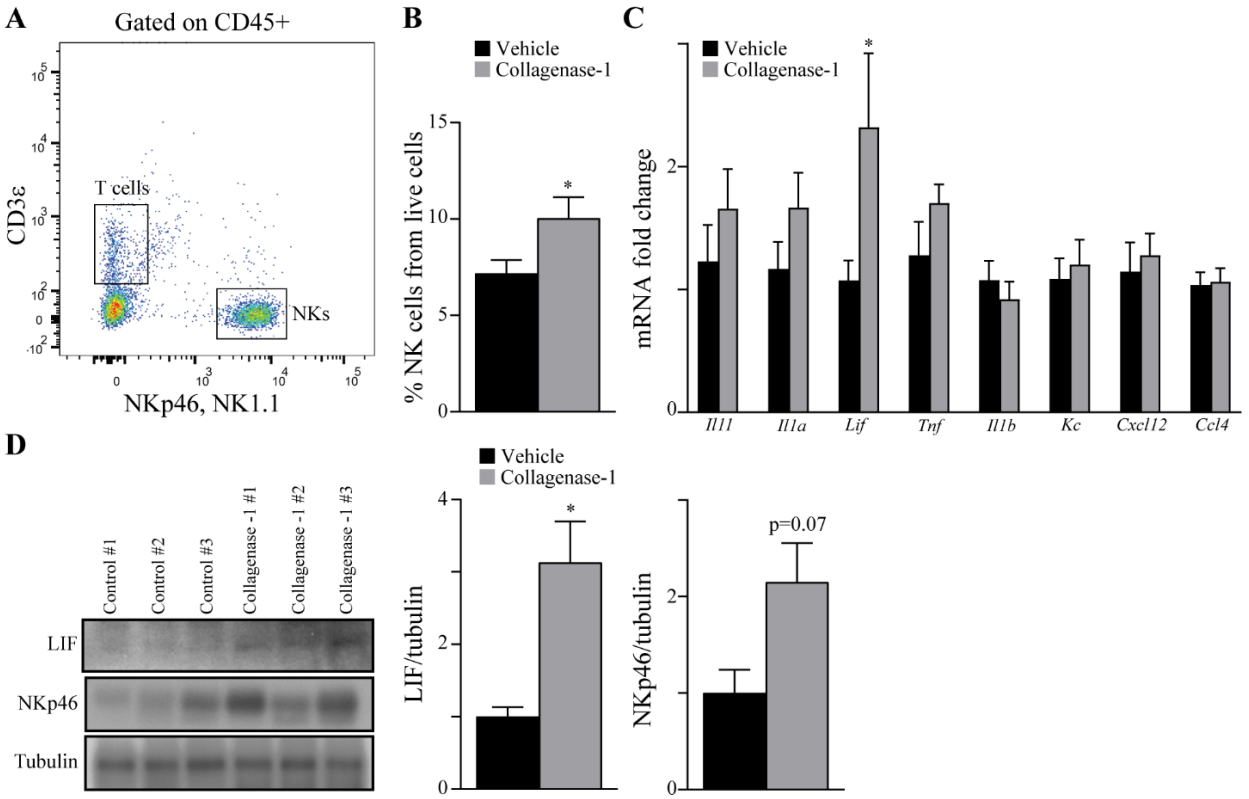

Fig. 6. Collagenase-1 induces upregulation of cytokine expression and NK cell infiltration in the spontaneous pregnancy model. (A) Representative flow cytometry images showing the gating strategy used to identify NK cells (CD45+CD3ε−NK1.1+NKp46+). **(B)** Quantification of flow cytometry results showing the percent of NK cells out of live cells at E4.5 (n ≥ 12). **(C)** Real-time PCR analysis of cytokines transcripts at E4.5 (n = 8). (**D)** Representative (left) and quantification (right) showing Western blot analysis of LIF and NKp46 expression in E4.5 implantation sites. Western blot quantification performed using ImageJ analysis tool (n = 3). NKs, Natural killer cells. Data was analyzed by an unpaired, two-tailed t-test. Results are presented as mean ± SEM with significance: *p < 0.05.

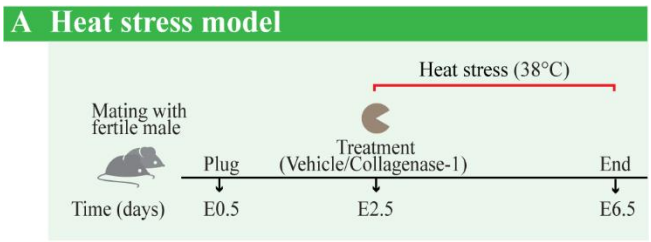

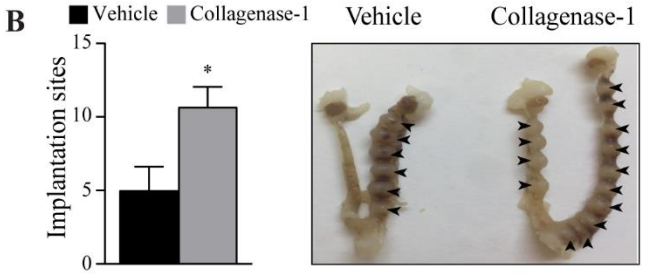

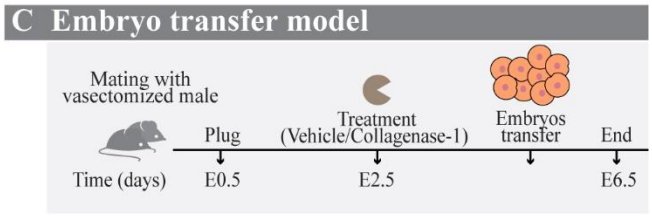

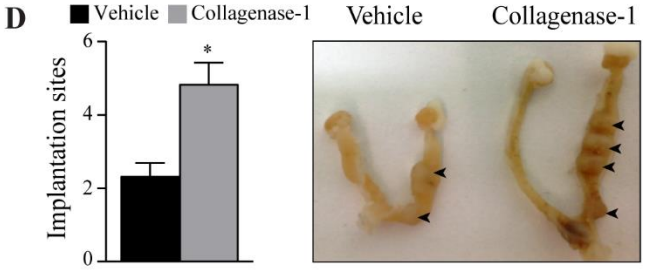

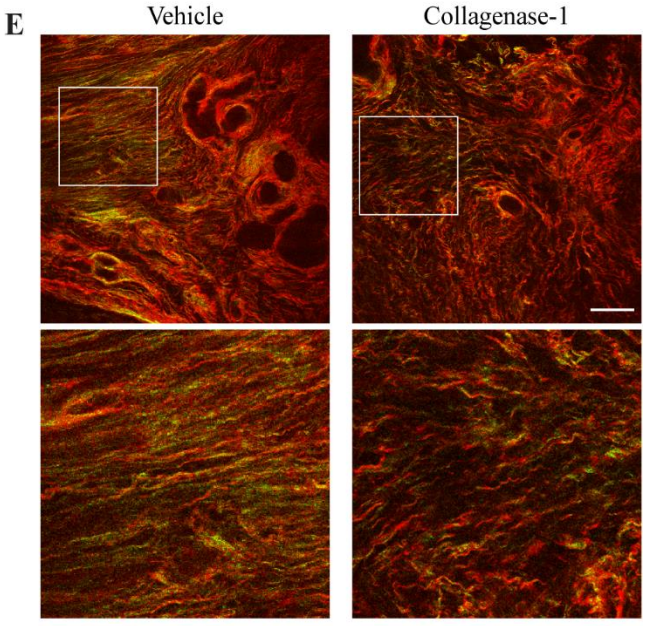

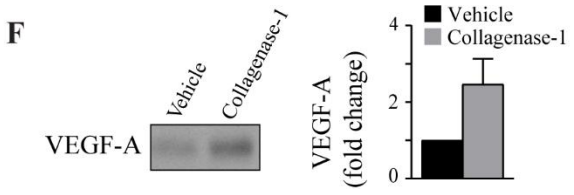

Fig. 7. Collagenase-1 improves implantation rate in embryo-transfer and heat-stress models and mechanistically affects human uteri-samples similarly to the mouse tissue. (A) A schematic representation of the heat-stress model. **(B)** Quantification of implantation sites and representative images of the uteri at E6.5 in the heat stress model. Arrowheads mark implantation sites (n = 9). **(C)** A schematic representation of the embryo transfer model. **(D)** Quantification of implantation sites and representative images of the uteri at E6.5 in the embryo transfer model. Implantation sites marked by arrowheads (n ≥ 15). **(E)** Representative SHG images of human uterine tissue sections either incubated with 5 nM of collagenase-1 or vehicle for 24 h (scale bar = 50 µm). **(F)** Representative Western blot of supernatants from decellularized human uterus samples that were incubated with collagenase-1 or vehicle for 24 h. Quantification of western blot analysis using ImageJ analysis tool (n = 3). Data was analyzed by an unpaired, two-tailed t-test. Results are presented as mean ± SEM with significance: *p < 0.05.

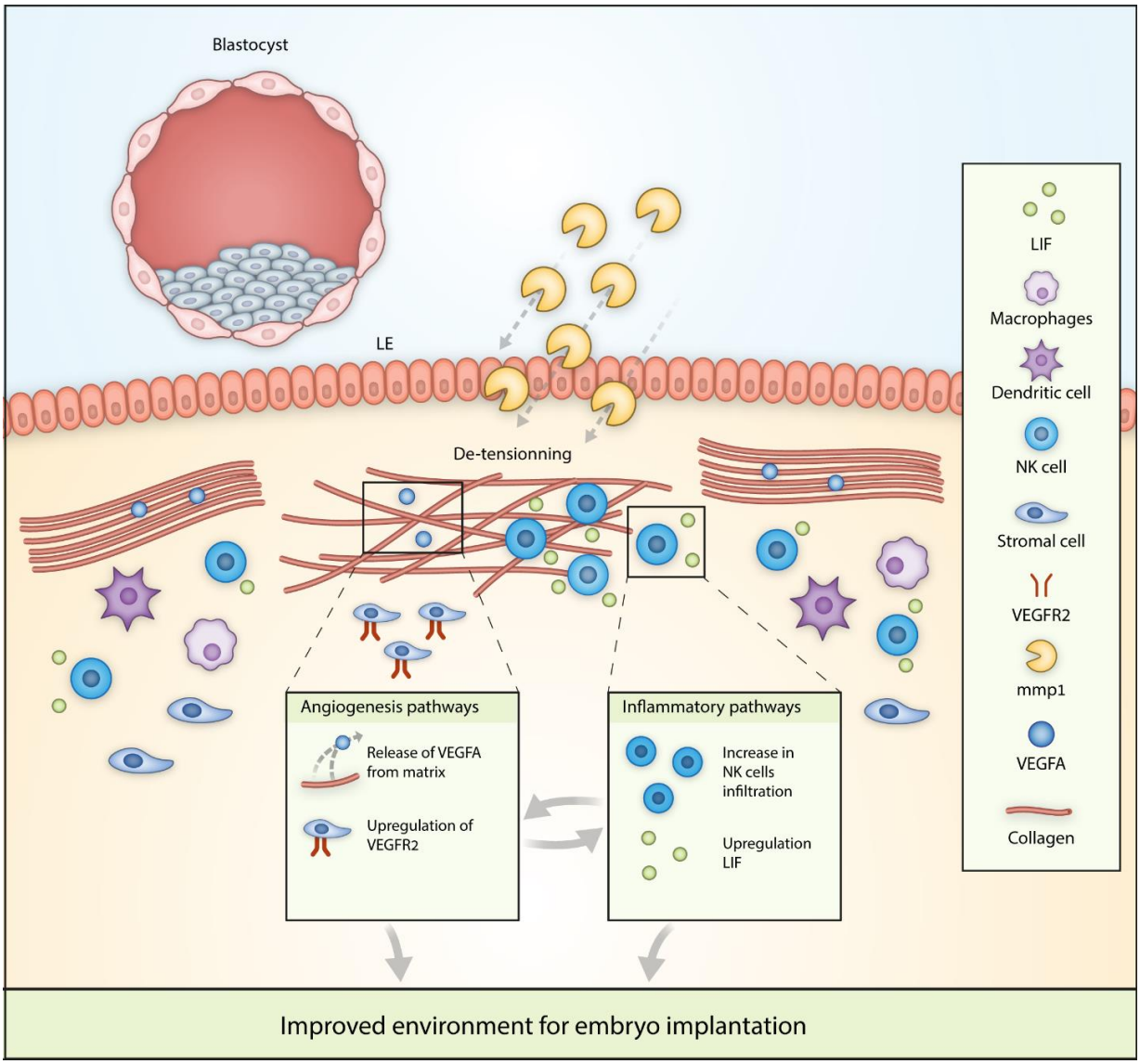

Fig. 8. Schematic representation of exogenous collagenase-1 mechanisms of action: Administering of collagenase-1 leads to de-tensioning of the dense collagen network, which in terns allows more accumulation of uNK cells that secretes LIF. In addition, collagenase-1 release VEGF-A from the uterus matrix and upregulates VEGFR-2 expression. These enhanced inflammatory and angiogenic pathways optimize the receptive environment for embryo implantation.